scientific reports

Check for updates

OPEN

Adipocyte-derived factors induce adherent to suspension transition in breast and pancreatic cancer cells through lipid metabolic alteration

Doru Kwon[1], Hyun Woo Park[2], Byung Soh Min[3] & Junjeong Choi[1]✉

Adipocytes play a dynamic role in the tumor microenvironment (TME) by acting as facilitators, providing cytokines and metabolites that regulate cancer progression and metastasis. Despite metastasis being a major contributor to cancer-associated mortality, our understanding of how adipocytes influence this process remains limited. This study aims to elucidate the regulatory mechanism of Adherent to Suspension Transition (AST) reprogramming within the adipocyte, driven by anchorage dependency. AST facilitates the conversion of adherent tumor cells into suspension cells, thereby contributing to the generation of circulating tumor cells (CTCs). We have evaluated generating AST cells from primary tumors using a dissemination assay that mimics CTCs in vitro. Additionally, we examined AST cell formation when incubated with human adipocyte-conditioned media (ADCM) using the InCucyte live-cell imaging system. Through this approach, we effectively assessed the impact of the tumor-adipocyte interactions on CTC formation from the perspective of AST. As a metastasis-initiating marker, CD36 is pivotal in fatty acid (FA) acquisition and regulates lipid metabolic remodeling during the AST. The generation of AST cells through AST reprogramming is controlled by fatty acid oxidation (FAO), and pharmacological blockade of CD36 and FAO significantly reduced AST cell generation. This demonstrates that CD36 plays a key role in the early stages of AST-induced dissemination. Additionally, promoting cancer cell aggressiveness through ADCM enhances metastatic potency and upregulates the expression of AST reprogramming factors. Inhibition of lipid metabolism not only suppresses AST cell formation but also decreases survival in suspension. This indicates that exogenous lipid uptake and FAO via CD36 play crucial roles in the metastasis process, facilitating the dissemination of primary tumors into the bloodstream. Adipocytes contribute to cancer progression by supplying various metabolites to cancer cells. While primary tumors predominantly rely on glucose as a major energy source, cellular remodeling during dissemination shifts metabolic dependency toward lipids. In the TME, where adipocytes are abundant, tumor cells acquire FA through CD36-mediated uptake for metabolic adaptation. This shift to lipid metabolism is essential for AST, and thus, targeting lipid metabolism via inhibition of CD36 and FAO could serve as a potential therapeutic strategy for AST.

Keywords Circulating tumor cell, AST, Tumor microenvironment, Adipocytes, Lipid metabolism, CD36

Abbreviations

TME	Tumor microenvironment
AST	Adherent to suspension transition
CTCs	Circulating tumor cells
CM	Conditioned media
ADCM	Adipocyte conditioned media
EMT	Epithelial to mesenchymal transition

[1]College of Pharmacy, Yonsei Institute of Pharmaceutical Sciences, Yonsei University, Incheon, Republic of Korea. [2]Department of Biochemistry, College of Life Science and Biotechnology, Yonsei University, Brain Korea 21 Project, Seoul 03722, Republic of Korea. [3]Department of Surgery, Yonsei University College of Medicine, Seoul, Republic of Korea. ✉email: junjeong@yonsei.ac.kr

IDCs	Invasive ductal carcinoma
ROS	Reactive oxygen species
FAO	Fatty acid oxidation
OCR	Oxygen consumption rate
ECAR	Extracellular acidification rate
TCGA	The cancer genome atlas
2-DG	2-Deoxy glucose
NCBI	National center for biotechnology information
qPCR	Quantitative polymerase chain reaction
SSO	Sulfo-N-sucinimidyl oleate

Background

In most cancers, metastasis is the leading cause of mortality[1]highlighting the critical need to understand its mechanisms and develop effective treatments. While previous research has focused mainly on cancer cell-intrinsic changes, it is now evident that tumor progression is also regulated by interactions with the tumor microenvironment (TME)[2,3]including adipocytes, fibroblasts, and macrophages[4–6]. Despite growing interest in these interactions, our understanding remains limited, making this an ongoing area of investigation. Furthermore, while the traditional understanding of metastasis has been based on epithelial-to-mesenchymal transition (EMT)[7]it has been reported that CTCs dynamically switch between epithelial and mesenchymal states in the context of anticancer therapy and disease progression[8]. In breast invasive ductal carcinomas (IDC), evidence suggests that E-cadherin is fundamental for promoting metastasis, as its decrease leads to increased invasion but reduces the number of CTCs and their proliferation and survival[9]. Furthermore, a study demonstrated that in major human breast cancer subtypes, invasive leader cells can be characterized by cytokeratin-14 and p63 during collective invasion. Knockdown of these two genes effectively suppressed collective invasion[10]. These findings demonstrate the importance of the epithelial phenotype during the process of metastasis.

To address metastatic processes that occur independently of EMT, a novel paradigm called Adherent to Suspension Transition (AST) has been proposed. This concept involves reprogramming the anchorage dependency of cancer cells to alter their cell fate, transitioning adherent cells into suspension cells[11]. Cells undergo differentiation to reach their respective fates, ultimately performing specialized functions. Yamanaka's research confirmed that cell fate is governed by gene expression, where four key factors induced mature embryonic fibroblasts to become induced pluripotent stem cells (iPSCs)[12]. Another mechanism of cell fate remodeling is EMT, where epithelial cells are reprogrammed into mesenchymal cells, resulting in decreased cell-matrix adhesion and the acquisition of migration and invasion properties[13]. However, since both epithelial and mesenchymal cells share adherent characteristics, our research team aimed to identify key factors that induce suspension ability, akin to blood cells[11]. We analyzed 148 adherent cells and 43 suspension cells from the Human ENCODE database to identify genes specifically expressed in suspension cells[11]. Since suspension properties are inherent to blood cells, we identified 20 blood cell-related genes from a pool of 2325 suspension-specific genes[11]. When ectopically expressed these genes, we observed that they induced suspension characteristics in HEK293A cells[11]. Through a stepwise selection process, we identified 10 blood cell-related genes: IKZF1, BTG2, NFE2, IRF8, SPIB, GATA1, KLF1, TAL1, IKZF3 and POU2F2, from the initial 20 genes[11]. Furthermore, we successfully identified the four key AST factors[11]. When ectopically expressed, IKZF1, BTG2, NFE2, and IRF8 induced a suspension phenotype not only in HEK293A cells but also in MDA-MB-231 cells[11]. This occurs through two mechanisms: #1 the downregulation of the Hippo pathway's YAP-TEAD signaling, leading to extracellular matrix remodeling, and #2 the reduction of reactive oxygen species (ROS) levels through hemoglobin genes HBA1 and HBA2, thereby enhancing suspension viability[11]. Furthermore, comparative analysis between primary tumors and CTCs in both in vivo models and patient samples revealed that the four key AST factors were distinctly expressed in CTCs[11]. Targeting these factors effectively suppressed metastasis, highlighting their potential for therapeutic intervention against metastasis[11]. AST exhibits characteristics expressed in the hematopoietic lineage and can regulate circulating tumor cells[11]. It has been shown to induce tumor cell dissemination independently of the epithelial and mesenchymal phenotypes[11].

Adipocytes have been studied for their role in cancer metastasis across multiple cancer types[4,14]However, they are critical in breast cancer[15]where the adjacent primarily consists of adipose tissue, leading to extensive interactions. Adipocytes are known to regulate cancer progression by providing adipokines and metabolites[16]. Co-culturing adipocytes and cancer cells induce lipolysis in adipocytes, which supplies FA to cancer cells and modulates their lipid metabolism[17–19]. The energy and metabolic byproducts produced during these processes drive structural and functional remodeling in cancer cells[16]. Furthermore, adipocyte-mediated chemotaxis enhances cancer cell invasion[17]. Studies on metastasis-initiating cells have also shown that CD36, a fatty acid transporter involved in exogenous lipid uptake, can serve as a marker[20]. Various studies involving adipocyte-cancer cell co-culture have demonstrated upregulated CD36 expression in cancer cells[17,21]indicating its involvement in adipocyte-mediated cancer cell regulation. Therefore, to address the role of adipocytes in AST regulation and their impact on metastasis, we aimed to elucidate their influence on the mechanisms underlying AST.

Herein, we extracted mesenchymal stem cells from human cancer-associated adipose tissue and differentiated them into mature adipocytes to explain an AST regulation in adipocytes context[22]. Additionally, we developed an in vitro model to mimic CTCs through a dissemination assay, enabling the generation of AST cells[23]. AST cells derived from adherent cells exhibit hematopoietic cell characteristics[11,23]. Accordingly, we established AST cells using ADCM and assessed AST efficiency in suspension state to evaluate the role of adipocytes in AST regulation. Furthermore, real-time monitoring of cell morphology changes using the IncuCyte live-cell imaging

system directly demonstrated the impact of adipocyte interactions on AST induction and formation, providing insights into how adipocyte-derived factors remodel cancer cell anchorage dependency. Understanding CTCs is essential for comprehending the mechanism of driving cancer metastasis. How adipocytes induce cancer cell dissemination via metabolic remodeling by promoting AST from the primary tumor could broaden our perspectives on cancer metastasis progression.

Materials and methods

Cell culture and drug treatments

The MDA-MB-231 and SUIT2 cell lines were sourced from ATCC. After thawing and initial culturing, the cells were passaged up to passage 20. Cells were maintained in RPMI medium supplemented with 10% FBS and 1% penicillin-streptomycin. As needed, the cells were treated with 200 μM CD36 inhibitor (Sulfo-N-succinimidyl oleate; Selleckchem, E2988), 20 μM FABP4 inhibitor (BMS309403; Selleckchem, S6622), 100 μM CPT1A inhibitor (Etomoxir; Medchemexpress, HY-50202), and 600 μM glycolysis inhibitor (2-deoxy-D-glucose; Medchemexpress, HY-13966).

Differentiation of human adipocytes

Primary adipocytes were derived from mesenchymal stem cells obtained from the subcutaneous adipose tissues as by-product of human patients with colon cancer, isolated as previously described by Lee[24]. The isolated primary adipocytes were maintained in DMEM F-12 medium until they reached full confluency. To induce adipogenic differentiation, cells were cultured in adipogenic differentiation medium consisting of 33 μM biotin, 100 nM dexamethasone, 100 nM insulin, 200 μM indomethacin, 17 μM pantothenic acid, 10 μg/mL transferrin, 2 nM triiodothyronine, 500 μM isobutyl methylxanthine (IBMX), and 1 μM rosiglitazone. After 17 days, the medium was replaced with an adipogenic maintenance medium containing 33 μM biotin, 17 μM pantothenic acid, 10 nM insulin, and 10 nM dexamethasone. Cells were maintained in this medium with media changes every four days until further analysis[17,25].

Differentiated adipocytes were rinsed with PBS and incubated in a complete medium for two days. Conditioned media were collected and centrifuged at 4 °C, and the supernatant was stored at − 20 °C until use.

ADCM was collected from mature human adipocytes and mixed at a ratio of 75% ADCM to 25% complete RPMI 1640 medium (containing 10% FBS and 1% penicillin-streptomycin). The mixture was then sterilized using a 0.22 μm pore size filter before being used for cell incubation. The collection of human tissues followed the guidelines and regulations approved by the Institutional Review Board of Severance Hospital, Yonsei University Health System (4-2022-0998).

Cell dissemination assay

MDA-MB-231 (3×10^5) and SUIT2 (3×10^5) cells were seeded in a six-well plate and cultured for three days. Upon reaching 100% confluence, the culture medium was replaced with complete media. After 72 h, the cell culture media were harvested, and AST cells were collected. ADCM from mature human adipocytes was used instead of a complete medium to generate AST cells using adipocytes. The AST cells generated during the dissemination assay were monitored using the InCucyte live-cell imaging system (Sartorius). To compare cell viability, CellTox™ Green cytotoxicity Assay Reagent (Sartorius, 4633) was added to the media at a 1:2000 dilution, and fluorescence was measured at 488 nm wavelength. Suspension cell numbers were quantified using ImageJ software (version 1.52, https://wsr.imagej.net/ij/) to measure cells per unit area.

Measurement of AST efficiency

To assess the effective maintenance of viability in a suspension state, AST cells harvested through the dissemination assay were transferred to an ultra-low-attachment plate (Corning, 3417) and maintained in suspension for 48 h. AST efficiency was determined by calculating the relative viability of adherent and suspension cells using the CellTiter Glo® 2.0 cell viability assay (Promega, G9241)[11].

RNA extraction and quantitative real-time PCR

RNA was extracted using the Universal RNA Extraction Kit (TaKaRa, 9767) following the manufacturer's instructions. Quantitative PCR (qPCR) was performed using the TOPreal™ One-Step RT-qPCR Kit (Enzynomics, RT432M). The analysis was conducted on the StepOne™ Plus Real-Time PCR System (Applied Biosystems). All primer sequences are provided in Supplementary Table S1.

Seahorse metabolic assay

Adherent cells and AST cells were seeded at a density of 2×10^4 cells/well in XF24 cell culture plates with or without ADCM. For adherent cells, seeding was performed 24 h prior to measurement to allow attachment. In contrast, AST cells were seeded and immediately centrifuged before measurement. Cells were subjected to the XF Cell Mito-Stress test (Agilent) following the manufacturer's instructions. Oxygen consumption rate (OCR) was measured to assess oxidative metabolism, while extracellular acidification rate (ECAR) was quantified to evaluate glycolysis. The OCR/ECAR ratio was used to compare oxidative phosphorylation to glycolysis. Investigative glucose, glutamine, and lipid metabolism, experiments were conducted with four groups: Glucose+/Glutamine+ (Glc+/Gln+), Glucose+ (Glc+), Glutamine+ (Gln+), and a nutrient-free condition. The Agilent Seahorse XF Mito Fuel Flex Test (Agilent, 103260-100) was performed to evaluate the dependence on glucose, fatty acid, and glutamine metabolism. To inhibit the oxidative metabolism of glucose, fatty acids, and glutamine, UK5099, Etomoxir, and BPTES were respectively applied according to the manufacturer's instructions. The OCR/ECAR ratio was compared across treatment groups to assess metabolic shifts. Each group was supplemented

with glucose, glutamine, or pyruvate accordingly using XF RPMI medium (Agilent, 103576-100), which lacks glucose, L-glutamine, and sodium pyruvate, as the base medium.

Data availability and visualization

References from The cancer genome atlas (TCGA) are available on the public cBioPortal website (https://www.cbioportal.org/). To examine the co-expression of lipid transport genes related to the 17 AST factors, we obtained the lipid transport gene set from the GSEA database (https://www.gsea-msigdb.org/gsea/index.jsp). We compared gene co-expression in 1108 breast invasive carcinoma samples and 186 pancreatic adenocarcinoma samples. Co-expression levels were determined using Spearman's correlation, and heatmap were generated using GraphPad Prism software (version 8, https://www.graphpad.com/features).

Intracellular lipid accumulation measurements

Intracellular lipid content in differentiated mature human adipocytes, adherent cells, AST cells was assessed using Oil Red O staining. For AST cells, attachment to the plate was aided by centrifugation at 1000 rpm for 5 min, followed by fixation with 4% paraformaldehyde at room temperature for 30 min. After three PBS washes (5 min each), cells were incubated with Oil Red O staining solution, filtered through a 0.22 μm membrane, and stained for 20 min. Following an additional three PBS washes, the staining solution was removed, and images were captured. Lipid content was quantified by extracting the stain with 100% isopropanol, incubating on a rotating shaker for 5 min, and transferring 200 μl of the solution to a 96-well plate. Absorbance was measured at 510 nm using a spectrophotometer (Tecan group limited).

Adherent cancer viability test

To assess the viability of adherent cancer cells after treatment with CD36 inhibitor, FABP4 inhibitor, CPT1A inhibitor, and 2-DG at different concentrations, cells were seeded at a density of 8×10^3 cells/well in triplicate in a 96-well plate. CD36 inhibitor, FABP4 inhibitor, and CPT1A inhibitor were administered at concentrations of 5μM, 10μM, 25μM, 50μM, 100μM, and 200μM. 2-DG was tested at 50 μM, 100 μM, 600 μM, 1 mM, 2 mM, 5 mM, and 10 mM. After 48 h, the EZ-CYTOX cell viability kit (Dogen, EZ-500) was added to each well (10 μl/well), followed by incubation at 37 °C for 2 h. Absorbance was measured at 450 nm using a spectrophotometer.

Flow cytometry

To assess CD36/AST co-expression, adherent cells, AST cells, and AST-ADCM cells were collected at a concentration of 3×10^6 cells/ml in PBS. Cells were fixed in 4% PFA at room temperature (RT) for 15 min, resuspended in 100 μl of 1% BSA in PBS, and incubated with primary antibodies against: CD36 (Protein tech, 18836-1-AP; Santacruz, SC-7309), IKZF1 (Cell Signaling Technology, D10E5), BTG2 (Abcam, ab197362), NFE2 (Abcam, ab140598), IRF8 (Atlas Antibodies, HPA002531), SPIB (Invitrogen, MA5-17179), BCL11A (Abcam, ab191401), GATA1 (Abcam, ab181544), EKLF/KLF1 (Abcam, ab175372), and TAL1 (Abcam, ab155195). After 1-h incubation at RT, cells were washed three times with ice-cold PBS then incubated with Alexa Fluor 488 or Alexa Fluor 647-conjugated secondary antibodies for 30 min. Initial cell selection was performed using FSC-A/SSC-A gating. All antibody information is provided in Supplementary Table S2.

*Gating strategy

FSC/SSC gating was used to remove debris and dead cells. Viable cells were selected using Live/Dead staining (PI staining).

Singlet discrimination was performed using FSC-H vs. FSC-A to exclude doublets.

Fluorescence compensation was applied using single-stained controls.

Thresholds for AST and CD36 expression were determined into isotype controls to account for background fluorescence.

Based on these criteria, cells were classified into four groups:

(1) AST-/CD36–.
(2) AST+/CD36–.
(3) AST-/CD36+.
(4) AST+/CD36+.

Migration and invasion assay

Corning Transwell inserts (8-μm pore size, Corning, 3464) were used for migration and invasion assays. For the invasion assay, inserts were coated with 1.0 mg/ml Matrigel (Corning, 354230). Adherent and AST cells were seeded at 1×10^4 cells/well in the upper chamber with 300 μl of serum-free media, while 700 μl of complete media was added to the lower chamber. Migration assays were assessed after 24 h, and invasion assays were evaluated after 48 h. Non-invading cells were removed by washing with PBS and staining with crystal violet solutin (Sigma-Aldrich, V5265). Migratory and invasive cells were counted in five random fields at 10× magnification.

Spheroid formation assay

Adherent and AST cells were seeded at a density of 6×10^3 cells/well in round bottom, ultra-low binding plates (Corning, 7007) and centrifuged at 1000 rpm for 5 min. After three days, individual spheroids were imaged using an Olympus BX53 microscope. To assess spheroid viability, each spheroid was dissociated into single cells using a pipette, and viability was measured using the EZ-Cytox viability assay kit (Dogen, EZ-500).

Statistical analysis

Experiments were conducted independently three times under identical conditions. Mean values are presented, and error bars represent the standard error of the mean (SEM). Graphs were generated using GraphPad Prism. Statistical significance between two groups was determined using Student's t-test, with significance thresholds as follows: $p \leq 0.05$ (one symbol), $p \leq 0.01$ (two symbols), $p \leq 0.001$ (three symbols), and $p \leq 0.0001$ (four symbols).

Results

Adipocyte-conditioned media promote adherent to suspension transition

We isolated mesenchymal stem cells from human cancer-associated adipose tissue. We differentiated them into mature adipocytes using differentiation media over 21 days, as confirmed by Oil Red-O staining of lipid droplets (Fig. 1A). ADCM was collected from mature adipocytes by replacing the cell culture media, then mixed at a 75% ADCM to 25% fresh culture media. This mixture induced AST through a dissemination assay (Fig. 1A, B). We utilized the IncuCyte live-cell imaging system to confirm AST cell formation in MDA-MB-231 and SUIT2 cells under dissemination assay and ADCM incubation. AST cells exhibited a round morphology (red arrow) compared to adherent cells. The results showed a significant increase in AST cell number following ADCM incubation (Fig. 1C, D, E, H).

The distinction between detached adherent cells and AST cells generated through the dissemination assay can be determined by differences in hematopoietic gene expression, including the four key AST factors and variations in suspension viability. Consequently, AST efficiency was quantified as the ratio of viable cells in suspension compared to adherent cells after detachment[11]. Adherent cells were prone to anoikis in suspension, whereas HEK293A cells expressing the four key AST factors-maintained viability. Additionally, HBA1 and HBA2 played a crucial role in anoikis resistance, as knockdown of these genes induced anoikis in suspension in HEK293A cells expressing the four AST factors[11]. To quantify AST efficiency, a dissemination assay was conducted to generate AST cells, followed by collecting equal numbers of adherent and AST cells, which were then cultured in suspension for two days on an ultra-low attachment plate and in vitro AST cells generated through the dissemination assay exhibited a significantly higher proportion of metabolically activated cells than adherent cells in suspension. Furthermore, ADCM incubation significantly increased the proportion of metabolically active adherent cells, with the highest proportion observed in AST cells. These findings demonstrate that suspension culture decreases viability, which is partially rescued by ADCM (Fig. 1F, I). ADCM incubation also enhanced anoikis resistance and metabolic activation in suspension culture. Additionally, HBA1 and HBA2 expression levels were significantly elevated in adherent and AST cells upon ADCM incubation (Fig. 1G, J). Since HBA1/2 are associated with blood cell traits, their role in CTCs involves ROS regulation to sustain suspension viability[11]. These results suggest that ADCM incubation enhances AST efficiency.

Due to the observed enhancement of AST formation and suspension viability following ADCM incubation, we investigated whether this also led to increased expression of the four key AST factors: IKZF1, BTG2, NFE2, and IRF8. The dissemination assay revealed a significant upregulation of these factors in MDA-MB-231 and SUIT2 AST cells upon ADCM incubation. Moreover, even in the adherent cells, a modest increase in expression was observed following ADCM incubation (Fig. 1K, L). Notably, NFE2 expression was significantly higher in AST-ADCM cells than in AST cells alone (Fig. 1K, L). Additionally, within a set of nine AST candidates including the four key AST factors, additional genes (SPIB, BCL11A, GATA1, KLF1, and TAL1) also exhibited increased expression upon ADCM incubation (Fig. S1A, B). These findings demonstrate that adipocyte interaction enhances AST formation, promotes suspension viability through upregulated anoikis resistance, and induces metabolic remodeling.

AST cells had increased oxygen consumption via lipid metabolic alterations

To investigate the mechanisms underlying AST enhancement through adipocyte interaction, we examined the metabolic influence of ADCM. ADCM contains various cytokines and metabolites that modulate cancer progression and metastasis[16,26–28]. Additionally, during CTC generation, adherent cells undergo cytoskeletal remodeling and metabolic shifts[29–31]. Metabolites and cytokines in ADCM play a critical role in facilitating this transition. Lymph node metastatic tumors within lipid-rich niches undergo a metabolic shift, where FAO becomes the primary energy source, surpassing glucose and glutamine metabolism[32]. Considering the metabolic activation of AST cells after ADCM incubation, we hypothesized that adipocyte-derived lipids serve as a major energy source for AST cells.

To assess cellular respiration, we measured the oxygen consumption rate (OCR) using Seahorse XF analysis. We quantified the extracellular acidification rate (ECAR) to evaluate glycolysis levels, providing a comprehensive metabolic assessment of AST cells. This approach facilitated a comprehensive evaluation of the metabolic changes in AST cells. Upon ADCM incubation, adherent cells exhibited a slight, though non-significant, increase in basal OCR and maximum respiration following Carbonyl cyanide 4-(trifluoromethoxy)phenylhydrazone (FCCP) stimulation. However, AST cells substantially increased basal OCR compared to adherent cells. Furthermore, maximum respiration rates in AST cells increased 1.7-fold and 4-fold compared to adherent cells. AST cells incubated with ADCM displayed significantly higher basal OCR and maximum respiration than AST cells alone (Fig. 2A, C). Since ECAR reflects glycolysis, we used OCR/ECAR ratio to assess glycolytic dependence. Notably, in both MDA-MB-231 and SUIT2 cells, AST formation led to a substantial increase in oxidative metabolism independent of glycolysis (Fig. 2B, D). These findings indicate that AST cells exhibit a higher basal metabolic rate than adherent cells and demonstrate significantly enhanced metabolic capacity and energy demand. Moreover, ADCM incubation markedly increased metabolic activity independent of glycolysis.

Next, we investigated which energy sources among glucose, glutamine, or lipids play a predominant role in the metabolic shift induced by AST formation and ADCM incubation. We measured the OCR/ECAR ratio after sequentially depleting each nutrient to determine this. Cells were divided into four experimental conditions:

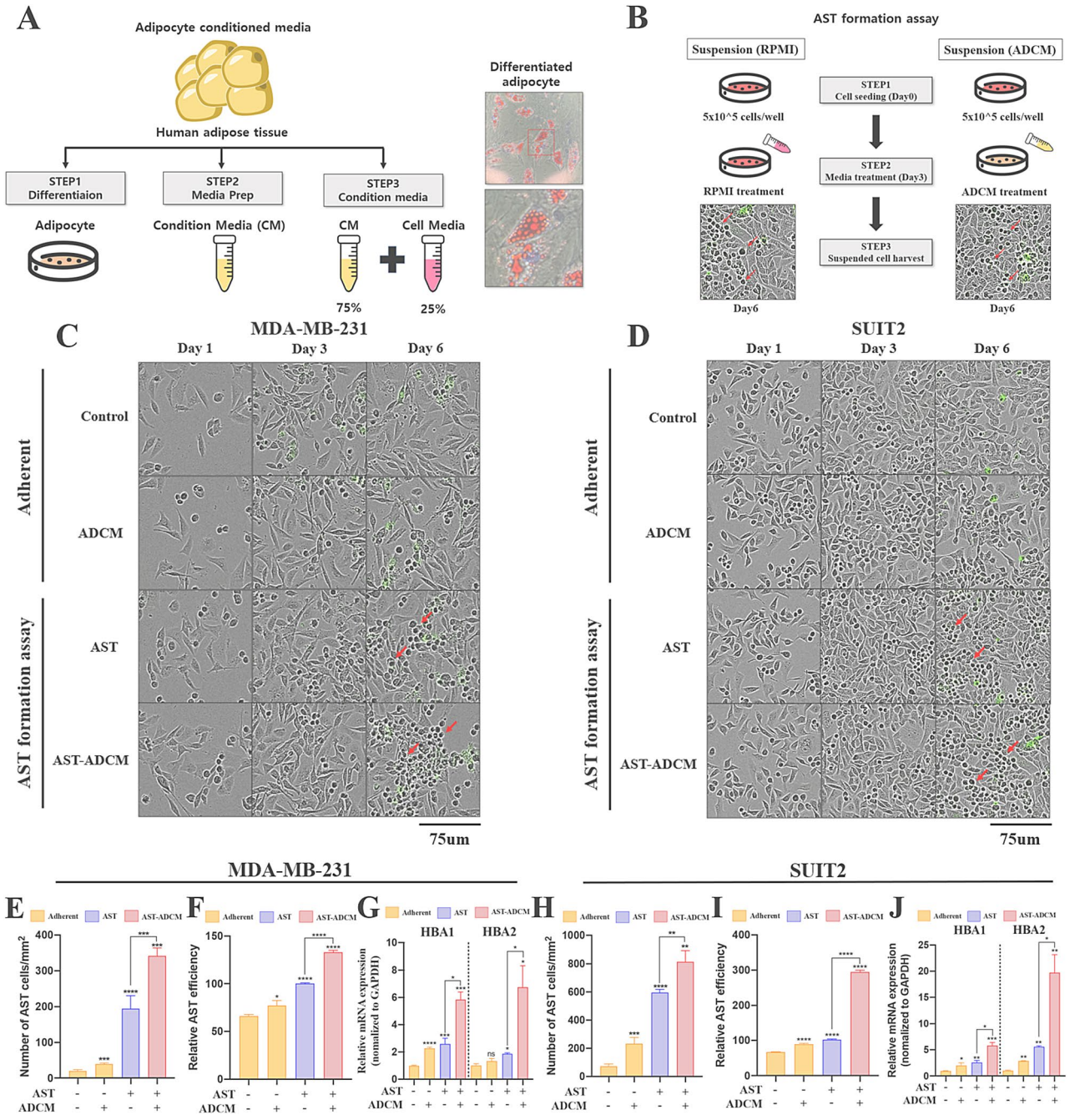

Fig. 1. Adipocyte-conditioned media promote adherent to suspension transition in MDA-MB-231 and SUIT2. (**A**) A schematic representation of ADCM extraction from human adipose tissue. Pre-adipocytes were isolated from human adipose tissue and differentiated into mature adipocytes. ADCM was used at a working concentration of 75% ADCM mixed with 25% complete RPMI 1640 medium for the dissemination assay. Illustration was created using BioRender (BioRender.com). (**B**) A diagram of dissemination assay and incubation with ADCM. After three days of culture, AST induction was performed using complete media or ADCM, respectively. Cells were harvested after 72 h of induction. (**C**, **D**) Live cell images of MDA-MB-231 and SUIT2 at different time points (days 1, 3, and 6). Red arrows indicated the AST cells. (**E**, **H**) Quantification of AST cells after cell dissemination assay in MDA-MB-231 and SUIT2 cultured with or without ADCM. (**F**, **I**) Quantification of AST efficiency of MDA-MB-231 and SUIT2 cultured with or without ADCM. Efficiency was measured by the CellTiter Glo® 2.0 cell viability assay after 2 days of culture in an ultra-low binding plate. (**G**, **J**) qRT-PCR was used to examine HBA1 and HBA2 expression in cell culture with or without ADCM and dissemination assay. (**K**, **L**) Quantifying mRNA expression levels of 4 key AST factors in MDA-MB-231 and SUIT2 culture with or without ADCM and dissemination assay. Relative mRNA expression was normalized to GAPDH. Data are presented as mean ± SD. Statistical significance was determined using Student's t-test. $^{****}p < 0.0001$; $^{***}p < 0.001$; $^{**}p < 0.01$; $^{*}p < 0.05$. All statistical comparisons were made against the control (adherent cells without ADCM). All images were acquired with magnification 10X, scale bar = 75 µm.

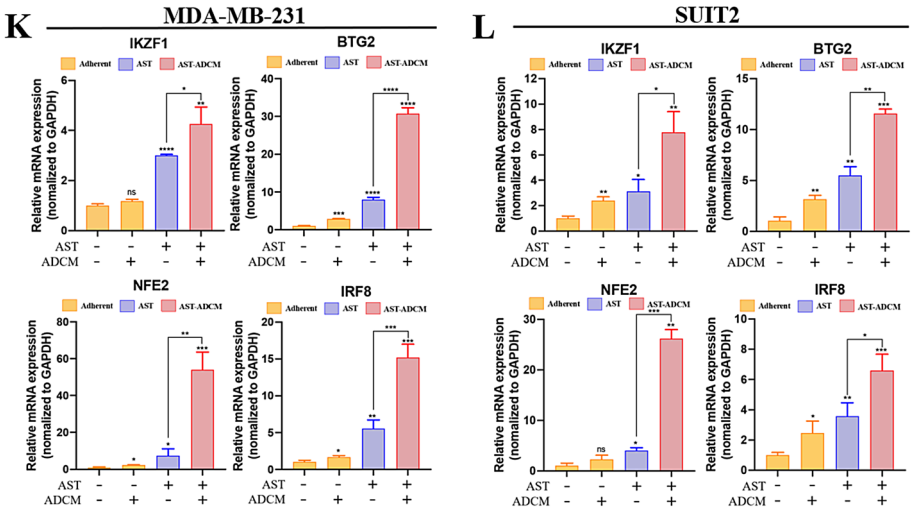

Fig. 1. (continued)

glucose+/glutamine+ (Glc+/Gln+), glucose+/glutamine– (Glc+/Gln–), glucose–/glutamine+ (Glc–/Gln+) and glucose–/glutamine– (Glc–/Gln–). By comparing the OCR/ECAR ratio across these conditions, we evaluated the impact of nutrient deprivation on OCR. This approach allowed us to investigate the distinct roles of nutrients in the observed metabolic changes[33]. In MDA-MB-231, adherent cells exhibited the lowest OCR/ECAR ratio in the Glc+/Gln + condition, indicating a strong reliance on glycolysis. Minimal OCR/ECAR changes were observed across other conditions, including Glc–/Gln–. Interestingly, ADCM incubation significantly increased the OCR/ECAR ratio in the Glc–/Gln– condition, suggesting a metabolic shift toward lipid metabolism (Fig. 2E). Similarly, in AST cells, the OCR/ECAR ratio increased significantly when glucose and glutamine were depleted compared to conditions where either nutrient was present. Furthermore, ADCM incubation strongly enhanced OCR in a glycolysis-independent manner (Fig. 2F). These findings suggest that AST cells exhibit reduced glucose dependency and an increased reliance on lipid metabolism in MDA-MB-231 cells. In SUIT2 cells, a slightly different metabolic pattern emerged. Adherent cells displayed a higher OCR/ECAR ratio under Glc–/Gln– conditions following ADCM incubation. Notably, AST cellsADCM incubation was shown to increase not only lipid metabolism but also the relative metabolic dependency on glutamine (Fig. 2G, H). We performed the XF Mito Fuel Flex Test to investigate further the oxidative metabolic dependencies on glucose, FA, and glutamine. This assay sequentially applies three metabolic inhibitors to assess reliance on each fuel source: UK5099 blocks mitochondrial pyruvate import, thereby inhibiting glucose oxidation. Etomoxir prevents fatty acid transport into mitochondria, inhibiting fatty acid oxidation. BPTES inhibits glutaminase (GLS), blocking glutamine metabolism and its mitochondrial entry. The results showed that after ADCM incubation, AST cells from MDA-MB-231 (Fig. 2I–K) and SUIT2 (Fig. 2L–N) exhibited a significant increase in FAO dependency. This finding further underscores the metabolic reprogramming induced by ADCM. These findings suggest that ADCM drives a metabolic shift in AST cells, promoting lipid utilization and enhancing their metabolic adaptability.

An upregulated lipid uptake pathway increases lipid accumulation in AST cells

In many cancers, including breast and pancreatic cancer, metastatic progression relies on energy supply from stromal cells, such as adipocytes, which provide fatty acids. We hypothesized that AST cells and ADCM incubation increased dependency on lipid uptake. To confirm this, we analyzed TCGA microarray data from 1108 breast invasive carcinoma and 186 pancreatic adenocarcinoma samples to examine the correlation between 17 lipid transport-related genes and AST genes. In breast-invasive carcinoma, ACSL5, CD36, and FABP4 exhibited positive correlations with AST genes (Fig. 3A). ACSL5 did not show a positive correlation in pancreatic adenocarcinoma, but CD36 and FABP4 demonstrated strong positive correlations (Fig. 3B). These findings suggest CD36 and FABP4, lipid transport genes, are closely associated with AST expression. Cancer cells acquire lipids through two primaries mechanisms: endogenous lipid synthesis and exogenous lipid uptake. To distinguish between these pathways, we measured the mRNA levels of FASN and SCD, key enzymes in endogenous lipid synthesis, and CD36 and FABP4, which are involved in exogenous lipid uptake. In MDA-MB-231 cells, FASN mRNA levels remained unchanged regardless of AST or ADCM incubation. However, SCD expressions increased in adherent and AST cells following ADCM incubation. Notably, SCD expression was not elevated in AST cells compared to adherent cells, suggesting that SCD is not a critical pathway in AST (Fig. 3C). Similar results were observed in SUIT2 cells, where ADCM incubation upregulated FASN expression but did not alter levels in AST cells compared to adherent cells (Fig. 3D). In contrast, MDA-MB-231 cells, FABP4 expression remained unchanged in AST cells, whereas CD36 expression significantly increased under both AST and ADCM incubation conditions (Fig. 3E). Likewise, in SUIT2 cells, CD36 mRNA levels showed an increasing trend in AST cells and following ADCM incubation (Fig. 3F). These results suggest that enhanced lipid metabolism in AST is primarily driven by exogenous lipid uptake via CD36.

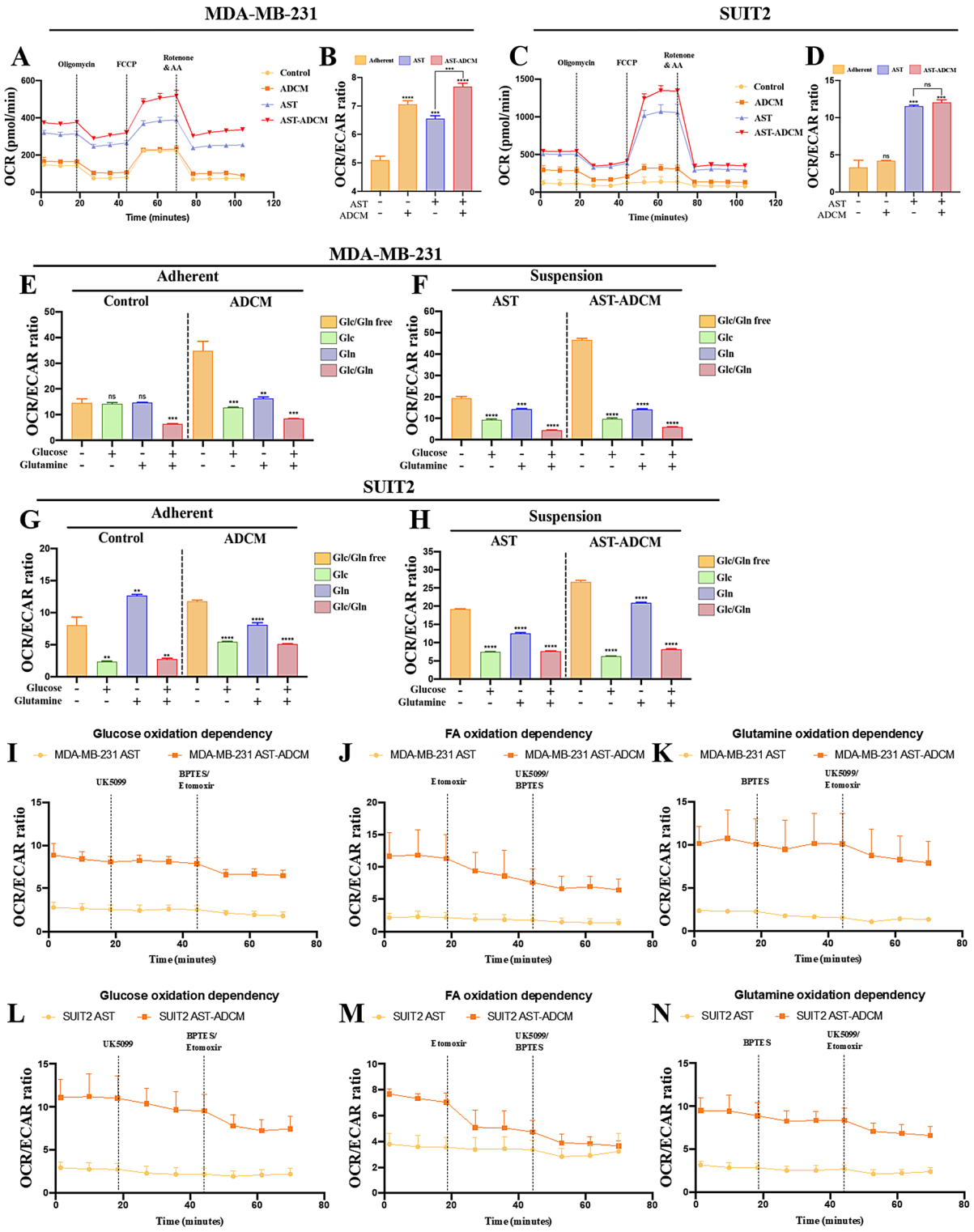

To assess whether lipid uptake is enhanced under AST and ADCM incubation in MDA-MB-231 and SUIT2 cells, we performed Oil Red O staining to measure intracellular lipid accumulation. In MDA-MB-231, lipid accumulation was significantly higher in AST cells than in adherent cells and elevated following ADCM incubation. To confirm that the increased lipid accumulation was mediated by fatty acid uptake, we treated cells with CD36 and FABP4 inhibitors, significantly reducing lipid content (Fig. 3G, H). Similar results were observed in SUIT2 cells, where lipid accumulation increased in both AST cells and following ADCM incubation but was substantially reduced upon treatment with CD36 and FABP4 inhibitors (Fig. 3I, J). These results indicate that AST increases exogenous lipid uptake through CD36 and FABP4 to meet its lipid demand, and ADCM incubation further facilitates this process by supplying lipids to cancer cells. Therefore, targeting CD36, FABP4, and broader lipid metabolism pathways may represent a potential therapeutic strategy for AST.

◀**Fig. 2**. AST cells showed increased oxygen consumption via lipid metabolic alterations in MDA-MB-231 and SUIT2. (**A**, **C**) The XFe24 seahorse oxygen consumption assay was carried out in MDA-MB-231 (**A**) and SUIT2 (**C**) cells with or without ADCM and dissemination assay. Each group was injected with the stressors oligomycin, FCCP, and rotenone/antimycin A (Rotenone/AA) into the media. (**B**, **D**) The ratio of OCR to ECAR was measured in MDA-MB-231 and SUIT2 cells. (**E** ~ **H**) The OCR/ECAR ratio alteration was assessed in both MDA-MB-231 and SUIT2 cells in both adherent and AST states. Values were measured upon individual or combined glucose and glutamine deprivation. Experiments were conducted with four groups: Glucose+/Glutamine+ (Glc+/Gln+), Glucose+ (Glc+), Glutamine+ (Gln+), and nutrient-free condition. (**I** ~ **N**) The XF Mito Fuel Flex test was performed in MDA-MB-231 and SUIT2 cells cultured with or without ADCM and subjected to a dissemination assay. Each group was sequentially treated with specific metabolic inhibitors: UK5099 (glucose metabolism inhibitor), Etomoxir (fatty acid oxidation inhibitor), and BPTES (glutamine metabolism inhibitor). To assess the dependency on each metabolic pathway, OCR and ECAR were first measured following the addition of each inhibitor alone. Subsequent changes in OCR and ECAR upon treatment with the remaining two inhibitors were then analyzed to evaluate the cells' metabolic sensitivity. Data are presented as mean ± SD. Statistical significance was determined using Student's t-test. $^{****}p < 0.0001$; $^{***}p < 0.001$; $^{**}p < 0.01$; $^{*}p < 0.05$. All statistical comparisons were made against the control group.

Sulfo-N-succinimidyl olate and BMS-309403 inhibit adherent to suspension transition

The inhibition of CD36 and FABP4 significantly reduced lipid uptake. To assess the impact of lipid supply inhibition on AST cell formation, we treated MDA-MB-231 and SUIT2 cells with CD36 inhibitor sulfo-N-succinimidyl olate and FABP4 inhibitor BMS-309403. Since AST cell formation is regulated by four key factors, IKZF1, BTG2, NFE2, and IRF8, we examined their mRNA expression following treatment with these inhibitors. In MDA-MB-231 and SUIT2 cells, treatment with a CD36 inhibitor (200 μM) and FABP4 inhibitor (20 μM) decreased the expression of four key AST factors, with a more pronounced reduction observed in AST-ADCM conditions (Fig. 4A, B). Co-treatment with both inhibitors did not further reduce AST factor expression in AST cells compared to individual treatments but showed more significant suppression in AST-ADCM conditions than single-drug treatment (Fig. 4A, B). Additionally, inhibition of CD36 and FABP4 significantly reduced the expression of five additional AST factors in MDA-MB-231 and SUIT2 cells (Fig. S2A, B). Furthermore, AST cells and ADCM incubation conditions exhibited reduced HBA1/2 mRNA expression following CD36 and FABP4 inhibition (Fig. 4C, D). Notably, in SUIT2 cells, NFE2 expression showed the most significant reduction upon dual inhibition (Fig. 4B). These findings suggest that targeting CD36 and FABP4 suppresses AST factor expression and reduces HBA1/2 mRNA levels, thereby impairing anoikis resistance.

Based on previous findings, AST primarily relies on lipid metabolism as a major energy source, acquiring essential FA through CD36 and FABP4-mediated uptake from the external environment. Given that inhibiting lipid uptake with CD36 and FABP4 inhibitors significantly reduced the expression of four key AST factors, we aimed to evaluate the impact of these drug treatments on AST cell formation and efficiency. Additionally, we investigated the effects of inhibiting FA β-oxidation by targeting CPT1A, transports responsible for delivering FA into the mitochondria. Using IncuCyte live-cell imaging in MDA-MB-231 and SUIT2 cells, we observed significant inhibition of AST cell formation following treatment with CD36, FABP4, and CPT1A inhibitors. Notably, CPT1A inhibition had the most pronounced effect, underscoring the critical role of β-oxidation in AST cell formation (Fig. 5A, C, K, M). In AST-ADCM, treatment with CD36 and FABP4 inhibitors reduced AST cell formation by approximately 50%, whereas CPT1A inhibition resulted in a more than 90% reduction (Fig. 5B, C, L, M). Given AST`s reduced reliance on glucose metabolism, we also treated cells with 2-Deoxy-D-glucose (2-DG) to assess its effect on AST cell formation. The results showed that inhibiting glycolysis did not significantly impact on AST cell formation in either MDA-MB-231 (Fig. S3A, C) or SUIT2 (Fig. S3B, D) cells. To further explore the relationship between FAO and AST formation, we tested whether AST formation was inhibited in a concentration-dependent manner upon CPT1A inhibition. MDA-MB-231 and SUIT2 cells were treated with Etomoxir at concentrations ranging from 10 to 100 μM, and AST formation was compared. A significant reduction in AST formation was observed at concentrations of 50 μM and above in MDA-MB-231 cells. In contrast, in SUIT2 cells, inhibition was observed from 20 μM onwards, reaching a substantial level (Fig. S3E ~ G). Moreover, when fresh media was replaced one day after CPT1A inhibitor treatment to allow for recovery, AST formation was restored to normal levels in both MDA-MB-231 (Fig. S3H, J) and SUIT2 (Fig. S3I, K) cells. These findings highlight the essential role of lipid metabolism in AST formation.

Next, we sought to assess AST efficiency changes following treatment with CD36, FABP4, and CPT1A inhibitors. To this end, adherent, AST, and AST-ADCM cells were cultured in suspension with drug treatment for 2 days, after which the ratio of metabolically active cells was measured. In MDA-MB-231 cells, the CD36 inhibitor reduced AST efficiency by approximately 50% in AST and AST-ADCM cells (Fig. 5D). The FABP4 inhibitor resulted in ~ 15% (Fig. 5E). While co-treatment with both inhibitors led to ~ 60% reduction (Fig. 5F). Notably, inhibition of FAO via CPT1A was the most effective, reducing AST efficiency by nearly 80% in both AST and AST-ADCM cells (Fig. 5G). In contrast, 2-DG treatment had no significant effect on AST efficiency (Fig. S3L). Similar trends were observed in SUIT2 cells, where CD36 and FABP4 inhibitors effectively reduced AST efficiency in both AST and AST-ADCM cells, with co-treatment leading to a further reduction (Fig. 5N ~ P). CPT1A inhibition exhibited potent suppression, reducing AST efficiency by over 90% in ADCM-AST cells (Fig. 5Q). However, 2-DG treatment did not affect AST efficiency (Fig. S3M). To investigate whether lipid metabolism inhibitors affected cell viability in adherent cells, we treated MDA-MB-231 and SUIT2 cells with varying concentrations of CD36, FABP4, and CPT1A inhibitors for two days. At concentrations of 200 μM for the CD36 inhibitor, 20 μM for the FABP4 inhibitor, and 100 μM for the CPT1A inhibitor, no significant impact

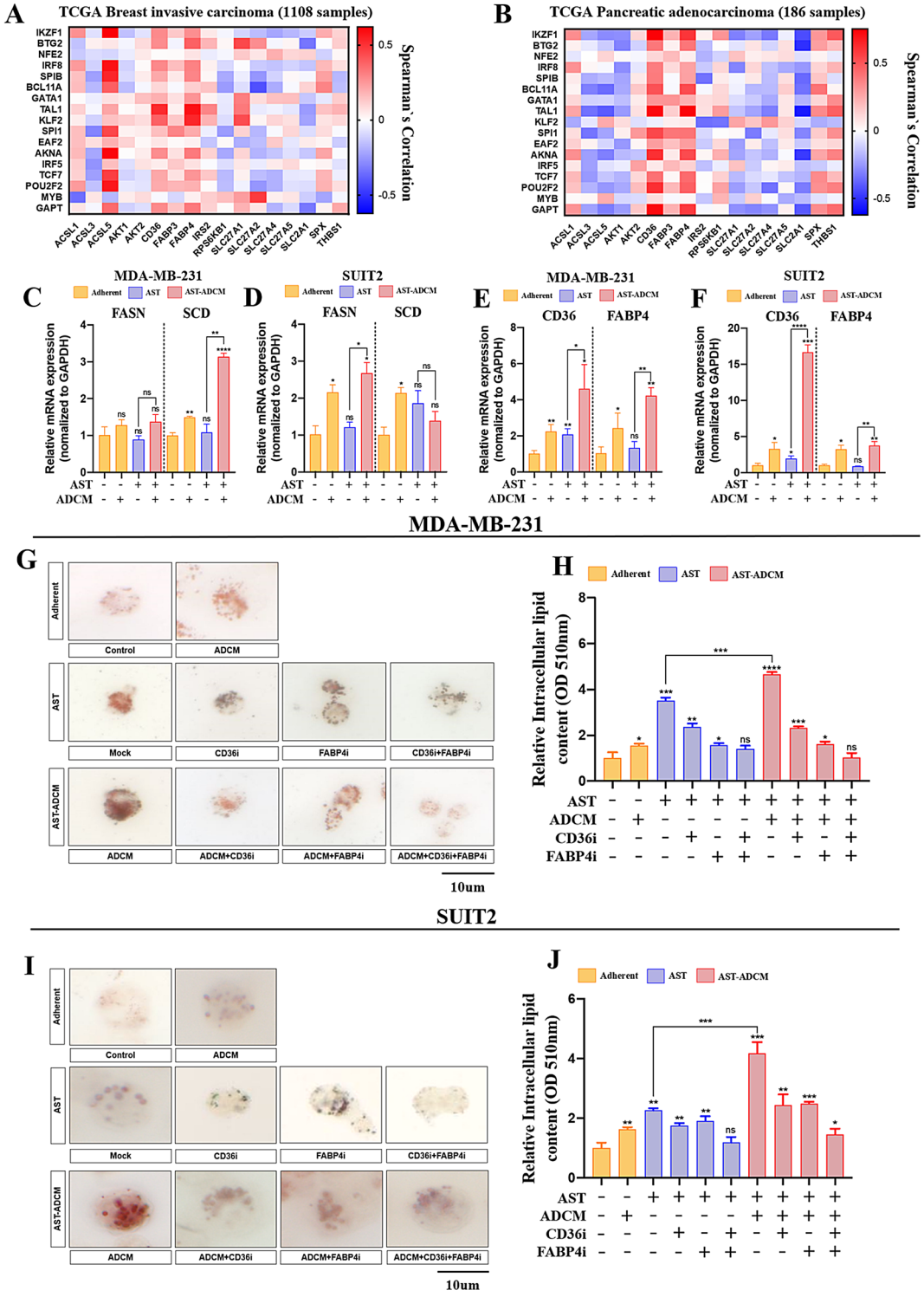

on viability was observed in either MDA-MB-231 (Fig. 5H ~ J) or SUIT2 (Fig. 5R ~ T) cells. However, when adherent cells were treated with 2-DG, cell viability decreased in a concentration-dependent manner in both MDA-MB-231 (Fig. S4A) and SUIT2 (Fig. S4B) cells. These results suggest that while adherent cells primarily rely on glucose metabolism for proliferation, they undergo metabolic shifts toward lipid utilization during AST induction. Further insights were gained through IncuCyte live-cell imaging. CPT1A inhibition had minimal impact on cell viability in MDA-MB-231 (Fig. S4C) and SUIT2 (Fig. S4D) cells over 48 h. However, when the CPT1A inhibitor was applied at the onset of AST induction, AST cell formation was completely blocked, and cell death ensued within 24 h in MDA-MB-231 (Fig. S4E) and SUIT2 (Fig. S4F) cells. Conversely, 2-DG treatment significantly inhibited cell proliferation in a concentration-dependent manner, as seen in MDA-MB-231 (Fig. S4G) and SUIT2 (Fig. S4H) cells. Interestingly, when 2-DG was administered at AST induction, no significant effect on AST formation or cell viability was observed in either MDA-MB-231 (Fig. S4I) or SUIT2 (Fig. S4J) cells. These findings demonstrate that CD36, FABP4, and CPT1A inhibitors effectively suppress AST efficiency

Fig. 3. An up-regulated lipid uptake pathway increases lipid accumulation in MDA-MB-231 and SUIT2. (**A**, **B**) TCGA micro-array mRNA expression data for breast invasive carcinoma (1108 samples in **A**) and pancreatic adenocarcinoma (186 samples in **B**) were used. Comparison was conducted between AST factors and a gene set related to lipid transport. Spearman's correlation was measured by comparing the data. (**C**, **D**) The mRNA levels of FASN and SCD involved in the endogenous lipid synthesis pathway were measured in MDA-MB-231 (**C**) and SUIT2 (**D**) cultures with or without ADCM and dissemination assay. (**E**, **F**) The mRNA levels of CD36 and FABP4 involved in the exogenous lipid uptake pathway were measured in MDA-MB-231 (**E**) and SUIT2 (**F**) cultures with or without ADCM and dissemination assay. (**G** ~ **J**) Oil-Red O staining was used to determine MDA-MB-231 and SUIT2 lipid accumulation. Sulfo-N-succinimidyl olate, a CD36 inhibitor, and BMS-309403, a FABP4 inhibitor, were used to inhibit exogenous lipid uptake in MDA-MB-231 (**G**, **H**) and SUIT2 (**I**, **J**) culture with or without ADCM and dissemination assay. Relative mRNA expression was normalized to GAPDH. Data are presented as mean ± SD. Statistical significance was determined using Student's t-test. $^{****}p < 0.0001$; $^{***}p < 0.001$; $^{**}p < 0.01$; $^{*}p < 0.05$. All statistical comparisons were made against the control (adherent cells without ADCM). All images were acquired with magnification 40X, scale bar = 10 µm.

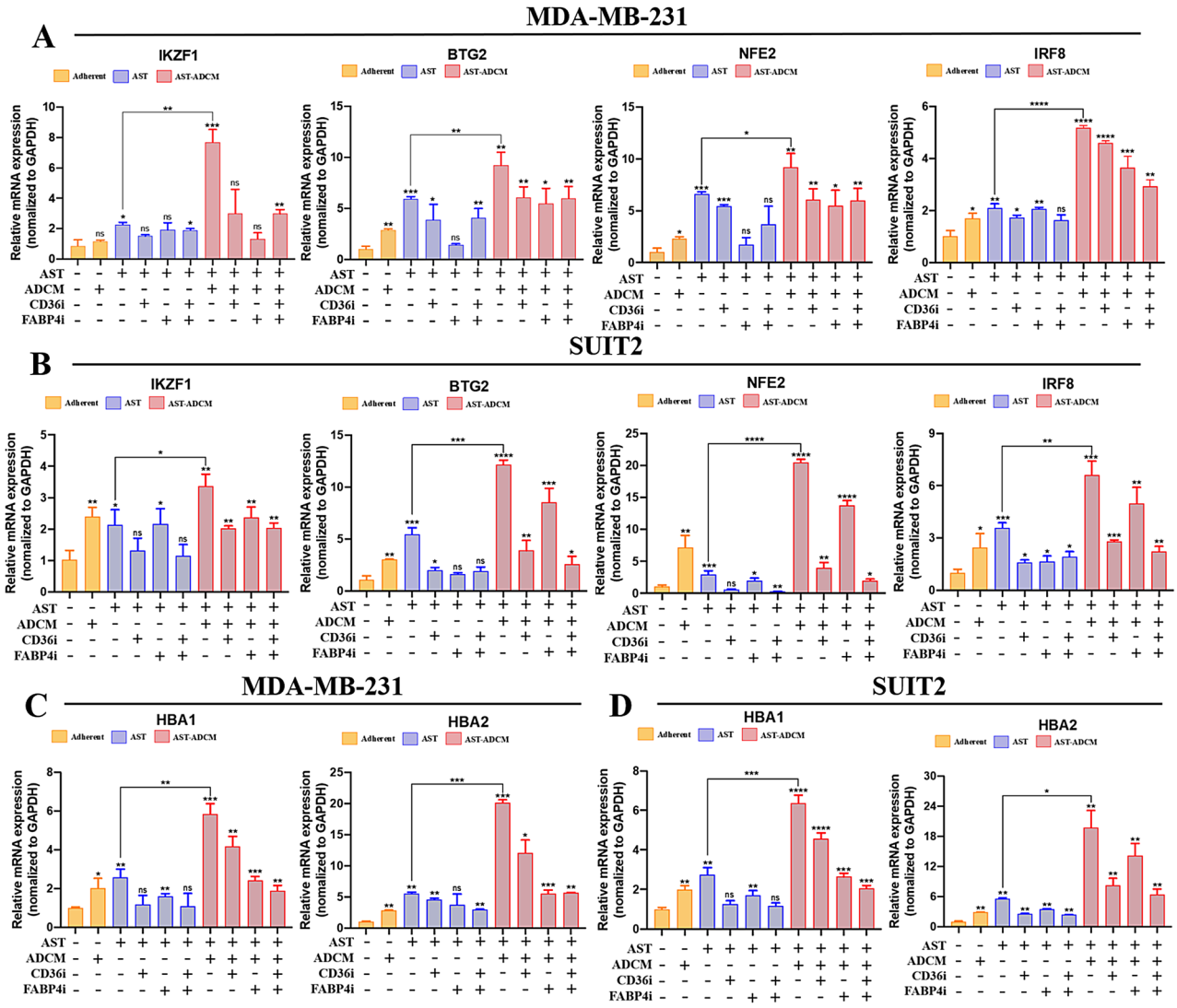

Fig. 4. Sulfo-N-Succinimidyl Olate and BMS-309403 decrease adherent to suspension transition factors in MDA-MB-231 and SUIT2. (**A** ~ **D**) The CD36 inhibitor Sulfo-N-Succinimidyl Olate and the FABP4 inhibitor BMS-309403 were used to compare four key AST factor expression and hematopoietic genes in MDA-MB-231 (**A**, **C**) and SUIT2 (**B**, **D**) cells based on exogenous lipid uptake inhibition. Relative mRNA expression was normalized to GAPDH. Data are presented as mean ± SD. Statistical significance was determined using Student's t-test. $^{****}p < 0.0001$; $^{***}p < 0.001$; $^{**}p < 0.01$; $^{*}p < 0.05$. All statistical comparisons were made against the control (adherent cells without ADCM).

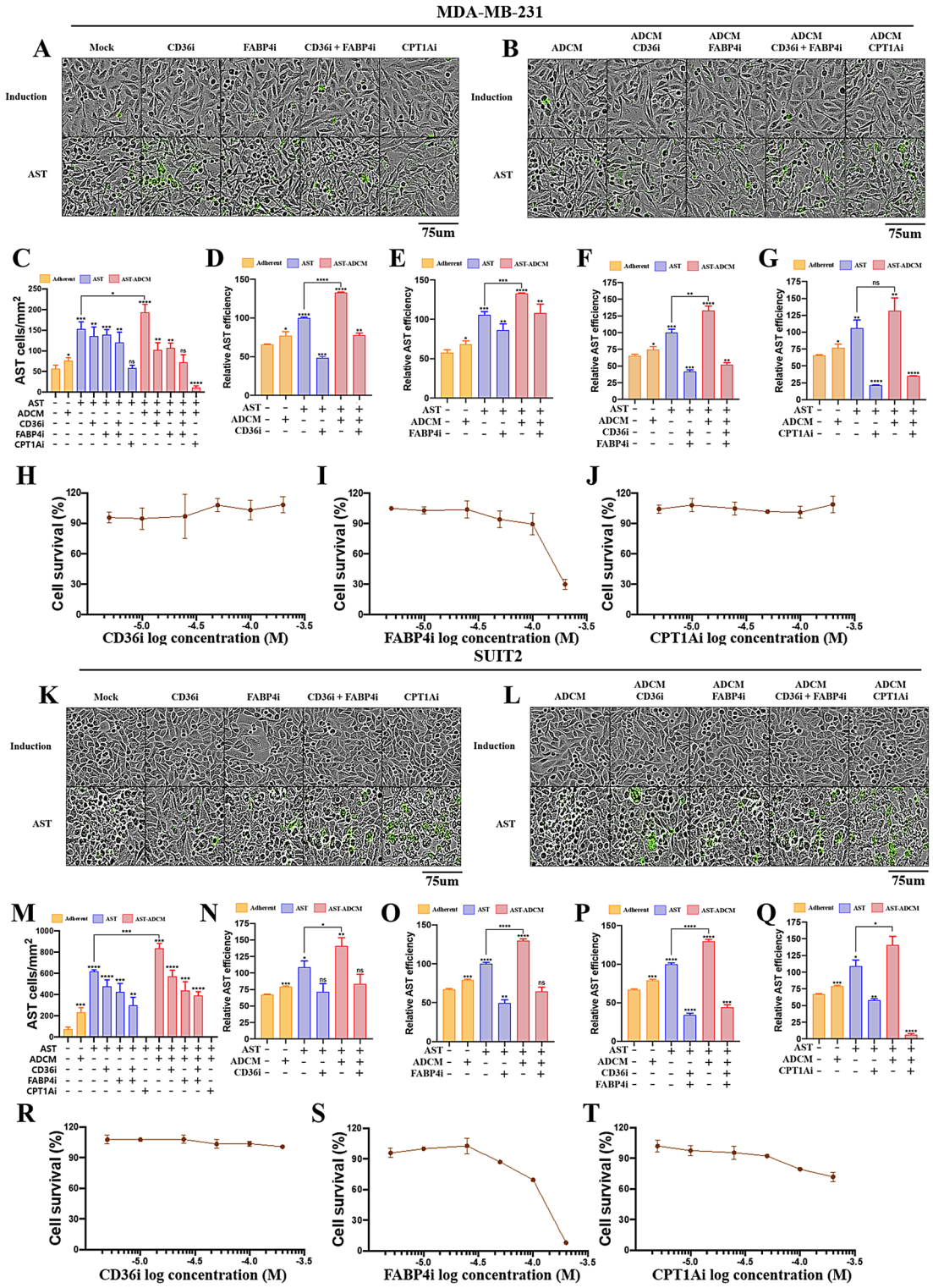

Fig. 5. Inhibition of fatty acid oxidation decreases adherent to suspension transition. (**A** ~ **C**, **K** ~ **M**) MDA-MB-231 (**A** ~ **C**) and SUIT2 (**K** ~ **M**) AST cell formations were observed when treated with CD36, FABP4, and CPT1A inhibitors in culture with or without ADCM and dissemination assay. (**D** ~ **G**, **N** ~ **Q**) AST efficiency was assessed in MDA-MB-231 (**D** ~ **G**) and SUIT2 (**N** ~ **Q**) culture with or without ADCM and dissemination assay when treated with CD36 inhibitor (**D**, **N**), FABP4 inhibitor (**E**, **O**), CD36 and FABP4 inhibitor (**F**, **P**), and CPT1A inhibitor (**G**, **Q**). (**H** ~ **J**, **R** ~ **T**) Cell viability measurements in MDA-MB-231 (**H** ~ **J**) and SUIT2 (**R** ~ **T**) cells after treatment with CD36 inhibitor (**H**, **R**), FABP4 inhibitor (**I**, **S**), and CPT1A inhibitor (**J**, **T**). Data are presented as mean ± SD. Statistical significance was determined using Student's t-test. $^{****}p < 0.0001$; $^{***}p < 0.001$; $^{**}p < 0.01$; $^{*}p < 0.05$. All statistical comparisons were made against the control (adherent cells without ADCM).

All images were acquired with magnification 10X, scale bar = 75 µm.

in both MDA-MB-231 and SUIT2 cells. Moreover, our results confirm that the inhibitor concentrations used do not adversely affect cell viability in adherent cancer cells, supporting their potential as therapeutic agents for preventing cancer dissemination.

CD36 as an AST-initiating cell marker, exhibits a positive correlation with AST

CD36 is implicated in FA uptake and as a marker for metastasis-initiating cells. It has been closely associated with EMT and stemness, as supported by multiple studies[17,20,21]. Given our previous findings demonstrating the effective inhibition of AST formation and AST efficiency through CD36 inhibition, we hypothesized a positive correlation between AST and CD36. Therefore, considering the potential mutual upregulation of AST and CD36, we aimed to investigate their relationship using flow cytometry. To examine this, we prepared adherent SUIT2, AST, and AST-ADCM cells. Co-staining of CD36 and AST markers was performed to assess changes in the proportion of CD36-positive cells relative to adherent cells. The results revealed a significant increase in AST-positive and CD36-positive cell populations for the four Key AST factors in AST and AST-ADCM cell groups compared to adherent cells (Fig. 6A ~ H). Five other AST factors also exhibited an increase (Fig. S5A ~ J). Over 80% of the CD36-positive population also expressed AST factors (Fig. 6I, Fig. S5K). These findings indicate an increase in the CD36-positive cell population in AST AST-ADCM cells, with a strong co-expression of AST factors. This further supports the role of CD36 as a key marker for AST-initiating cells.

Inhibition of AST-induced metastasis by pharmacological targeting of lipid metabolism

To confirm the essential role of AST in metastatic dissemination, our research team observed the transition of adherent cells to suspension cells following ectopic expression of AST factors in a breast cancer model. Furthermore, we confirmed the formation of CTCs through AST in NOD/SCID gamma (NSG) mice[11]. Additionally, our experiments using an AST knockdown cell line generated via shRNA demonstrated a significant reduction in breast cancer metastasis to the lung[11]. Considering the metabolic shift toward lipid metabolism during AST cell formation, we hypothesized that inhibiting lipid uptake, and metabolism could reduce AST-induced metastasis. We prepared adherent, AST, and AST-ADCM cells to investigate these hypotheses, followed by migration and invasion assay. Each cell type was cultured in suspension for two days and treated individually with a CD36 inhibitor, a CPT1A inhibitor, and 2-DG. We then quantified cell migration over 24 h using trans-

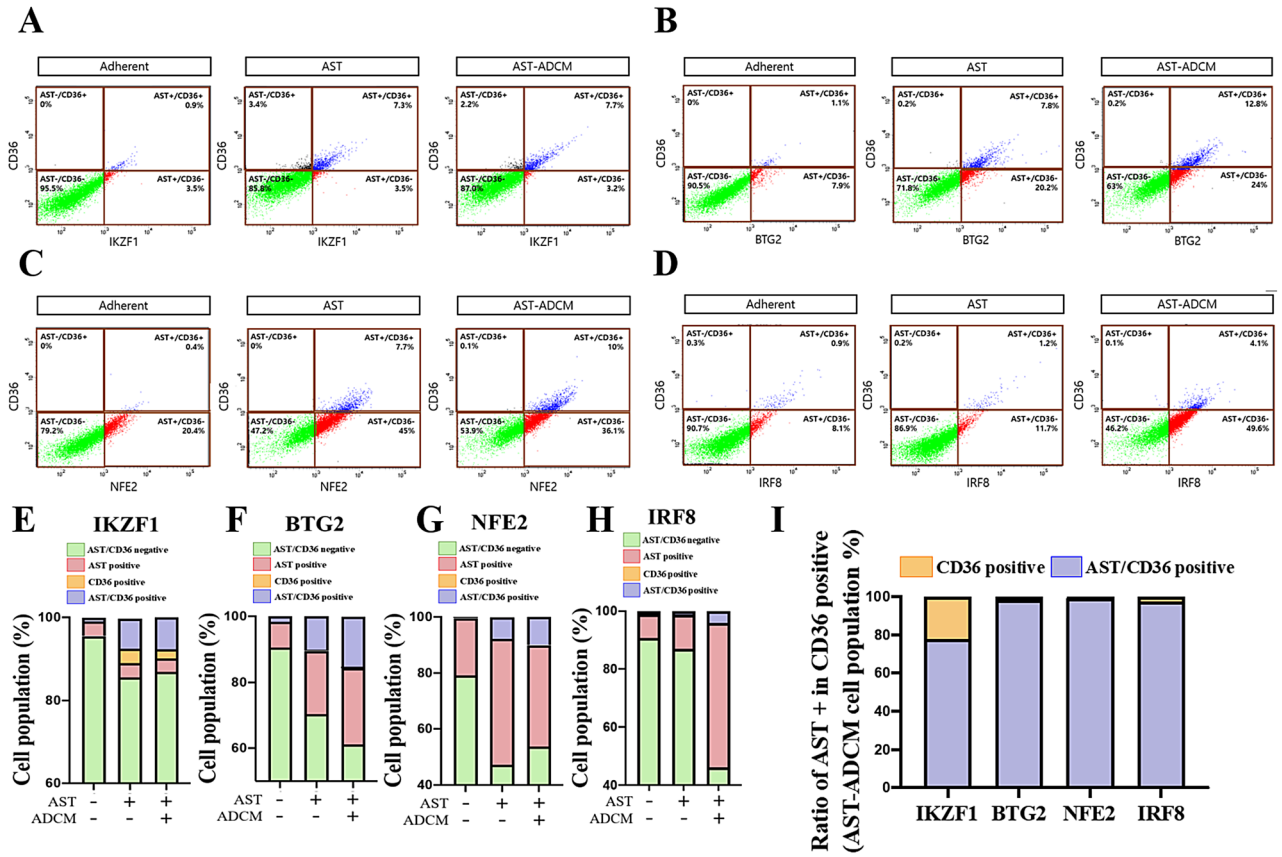

Fig. 6. CD36 has a positive correlation with four key adherent to suspension transition factors. (**A** ~ **H**) Flow cytometry was performed to compare CD36 to AST factor expression in SUIT2 cell culture with or without ADCM and dissemination assay. They were separated and measured into AST - / CD36 -, AST + / CD36 -, AST - / CD36 +, and AST + / CD36 + groups based on the AST factor and CD36 expression. (**I**) Quantitative measurement of the AST + /CD36 + cells in total CD36 + cells according to the AST cells with ADCM.

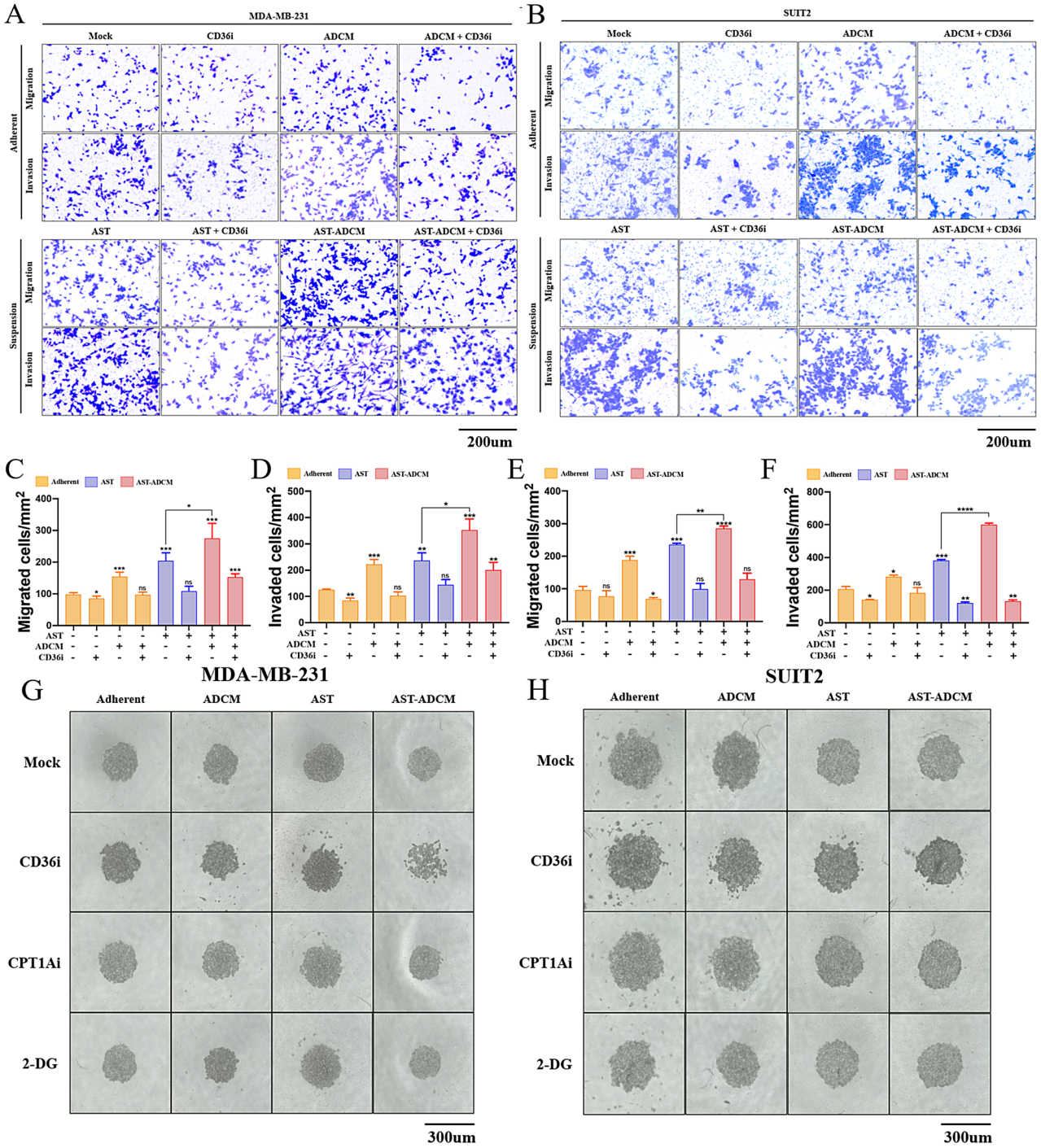

Fig. 7. Inhibition of fatty acid uptake leads to a reduction in the metastatic ability of AST. (**A**, **B**) Migration and invasion were measured in adherent and AST cells of MDA-MB-231 (**A**) and SUIT2 (**B**) when the CD36 inhibitor was treated. (**C** ~ **F**) MDA-MB-231 (**C**, **D**) and SUIT2 (**E**, **F**) migrated and invaded cells after being treated with CD36 inhibitor were quantified. (**G**, **H**) Spheroid formation assay was performed in MDA-MB-231 (**G**) and SUIT2 (**H**) cells. To assess the impact of metabolism inhibitors on spheroid cluster formation, CD36i, CPT1Ai, and 2-DG were individually administered. (**I**, **J**) Measurement of spheroid viability in MDA-MB-231 (**I**) and SUIT2 (**J**) cells upon treatment with metabolism inhibitors. Data are presented as mean ± SD. Statistical significance was determined using Student's t-test. $^{****}p < 0.0001$; $^{***}p < 0.001$; $^{**}p < 0.01$; $^{*}p < 0.05$. All statistical comparisons were made against the control. **A**, **B** were acquired with magnification 5 X, scale bar = 200 µm. **G**, **H** were acquired with magnification 10 X, scale bar = 300 µm.

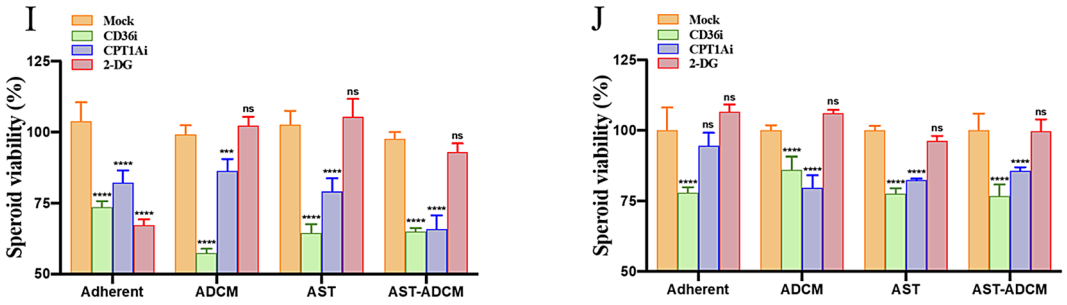

Fig. 7. (continued)

well assay and cell invasion over 48 h using Matrigel-coated trans-well, with ImageJ software for analysis. In MDA-MB-231 cells, migration increased 1.5-fold when incubated with ADCM, 2-fold in AST cells, and 2.5-fold in AST-ADCM cells (Fig. 7A, C). Treatment with the CD36 inhibitor led to a migration reduction of less than 10% in adherent cells, while AST and AST-ADCM cells exhibited a 30–50% reduction (Fig. 7A, C). Similarly, treatment with the CPT1A inhibitor resulted in a 60–70% reduction in AST and AST-ADCM cells (Fig. S6A, C). Conversely, inhibiting glycolysis had no significant effect on migration (Fig. S6G, I). Comparable results were observed in the invasion assay, where AST and AST-ADCM cells showed over a 40% reduction upon CD36 inhibition (Fig. 7A, D). The CPT1A inhibitor had a more profound effect, reducing invasion by ~80% (Figure S6 A, D). However, glycolysis inhibition had no impact (Fig. S6G, J). In SUIT2 cells, treatment with the CD36 inhibitor had no significant effect on migration in adherent cells, whereas AST and AST-ADCM cells exhibited over 50% reduction (Fig. 7B, E). In the invasion assay, adherent cells showed only ~15% reduction, whereas AST and AST-ADCM cells displayed a more substantial decrease (Fig. 7B, F). The CPT1A inhibitor effectively suppressed migration and invasion in AST and AST-ADCM cells but had minimal impact on adherent cells (Fig. S6B, E, F). Conversely, 2-DG treatment did not significantly affect migration or invasion (Fig. S6H, K, L). These results suggest that AST-induced AST cells possess a higher metastatic potential than adherent cells and that ADCM enhances migration and invasion. Moreover, CD36 and CPT1A inhibitors effectively suppressed migration and invasion in AST and AST-ADCM cells. The data also indicate that ADCM incubation reduces glucose dependency and increases reliance on lipid metabolism, contributing to AST-induced metastasis.

The formation of CTC clusters depends on cell-cell interactions involving junction proteins such as Plakoglobin, CD44, and ICAM1. In AST, anchorage dependence is regulated by cell-ECM junctions, while intercellular junctions remain unaffected. E-cadherin expression has been reported in AST cell interaction[11]. This suggests that in AST cells, changes in cell junctions primarily occur in the cell-matrix context rather than between cells. Given the reported link between CD36, Plakoglobin, and ICAM1 expression[34,35]we aimed to determine whether lipid metabolism-targeting inhibitors reduce AST-induced CTC cluster formation. To investigate this, we performed a spheroid formation assay using adherent, AST, and AST-ADCM cells. Spheroids (cell clusters) were treated with a CD36 inhibitor, CPT1A inhibitor, or glycolysis inhibitor (2-DG) for two days, and their formation and survival were assessed. Spheroid formation measurements showed that adherent, AST, and AST-ADCM cells formed comparable clusters under identical conditions with no significant differences. However, while CPT1A inhibition and 2-DG treatment had no discernible impact on spheroid formation, CD36 inhibition significantly reduced cluster formation. Remarkably, the adherent MDA-MB-231 cells showed minimal response to CD36 inhibition, whereas AST cells and, particularly, AST-ADCM cells exhibited strong inhibition, preventing the development of cluster cores (Fig. 7G). Spheroid viability measurements revealed that CD36 and CPT1A inhibitors reduced cell survival, whereas 2-DG only decreased viability in adherent cells (Fig. 7I). These findings suggest that co-culturing ADCM with breast cancer cells reduce glucose dependency and shifts metabolic reliance toward lipids. In SUIT2 cells, the results were slightly different. AST and AST-ADCM cells exhibited stronger cluster formation than adherent cells. CPT1A inhibition and 2-DG had minimal effects on clustering, while CD36 inhibition reduced cluster formation, though less dramatically than in MDA-MB-231 (Fig. 7H). Viability assays in SUIT2 showed only minor reductions upon drug treatments, but CD36 and CPT1A inhibitors significantly reduced viability in AST and AST-ADCM cells (Fig. 7J). Additionally, we assessed mRNA expression levels of Plakoglobin and VCAM1, both involved in CTC cluster formation. AST and AST-ADCM cells exhibited increased expression of these junction proteins, which were effectively suppressed by CD36 inhibition in both MDA-MB-231 and SUIT2 cells (Fig. S7A ~ D). In conclusion, lipid metabolism-targeting drugs decreased spheroid viability and effectively inhibited cluster formation in breast cancer cells.

Discussion and conclusions

Cancer metastasis is the process by which cancer cells migrate from the primary tumor to secondary sites, requiring the acquisition of new characteristics that facilitate their movement[36]. Previous studies have sought to explain cancer cell migration and invasion through the EMT theory[7,13]. However, theory alone does not fully capture the complexity of metastasis[8–10]. To address these gaps, research has shifted toward understanding anchorage dependency reprogramming and the mechanisms governing circulating tumor cell formation. The adherent-to-suspension transition (AST) theory has been proposed in this context.

From the AST perspective, it is postulated that AST factors are not expressed in solid tumors and do not arise from genetic mutations[11,23]. Instead, their expression is regulated by microenvironmental stressors[23]. These

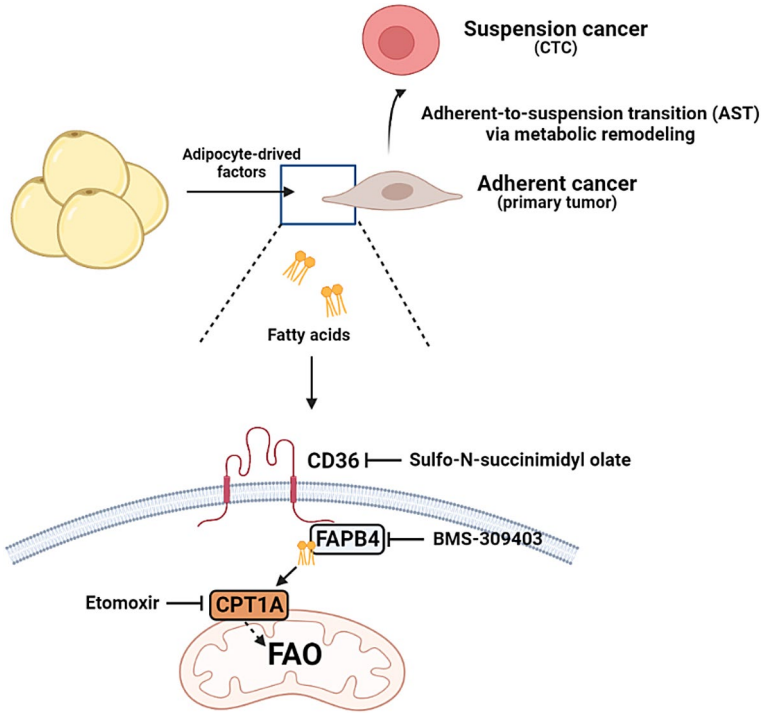

Fig. 8. Pharmacological targeting of lipid metabolism inhibits adherent to suspension transition. FA supplied by adipocytes is absorbed by cancer cells via the CD36 transporter. The FA delivered into mitochondria through CPT1A contributes to fulfilling the metabolic requirements of cancer cells through fatty acid oxidation. The increase in lipid metabolism through lipid metabolic alterations triggers the adherent to suspension transition. This transition can be effectively inhibited by antagonists targeting CD36, FABP4, and CPT1A, which are involved in this process. Illustration was created using BioRender (BioRender.com).

stressors increase the expression of AST factors, enhance cellular plasticity, and ultimately regulate cell-matrix anchorage dependency, thereby promoting cell dissemination[11,23]. Among these stressors, adipose tissue plays a particularly crucial role in various cancers, including breast cancer, as it shapes the TME and supplies key factors such as FAs and adipokines[14–16]. While several studies have explored the role of adipocytes in regulating metastasis[4,14–16]the mechanisms by which adipocytes control cellular anchorage dependency remain poorly understood. To address this knowledge gap, we developed an incubation model using ADCM extracted from human cancer-associated adipose tissue. Utilizing an in vitro cell dissemination assay, we demonstrated that interaction with adipocytes acts as a mechanical cue, increasing AST factor and effectively modulating cellular plasticity. Importantly, this regulation occurs independently of genetic mutations, providing evidence for non-mutational cue-mediated cellular changes.

As energy storage organs, adipocytes supply cancer cells with metabolites to fulfill their energy demands[14–16]. Metastatic colorectal and breast cancer patients exhibit higher serum lipid concentrations than non-metastatic patients[37,38]. CTCs increase their survival during circulation by uptaking exogenous lipids through CD36[39]. Furthermore, inhibiting FAO by silencing CPT1A leads to ROS accumulation, reducing CTC survival and migration ability[40]. These findings highlight the significance of lipid metabolism in CTC properties. Our cell dissemination assays, and adipocyte interaction experiments consistently revealed an increased metabolic demand in AST, shifting from glucose reliance to lipid dependency. While glucose serves as the major energy source in the primary tumor[41]AST induction triggers metabolic reprogramming, favoring lipid metabolism as the primary energy source. Additionally, identifying CD36 as a marker of AST-initiating cells sheds light on how AST is regulated through CD36, positioning it as a potential therapeutic target for adipocyte-induced metastasis.

Among the four key AST factors, NFE2 showed the most pronounced change in the AST-ADCM model. NFE2 is a known transcriptional regulator of globin genes expression required for hemoglobin synthesis and plays a crucial role in erythrocyte and platelet differentiation[42]. Additionally, NFE2 is involved in the KEAP1-NRF2 pathway, which regulates oxidative stress by stabilizing NRF2 and reducing oxidative damage[43]. Given that previous studies have demonstrated that anoikis resistance in AST is regulated by ROS[11]the observed increase in NFE2 expression by adipocytes may enhance anoikis resistance by modulating oxidative stress.

AST-induced metastasis reprograms cell-matrix interactions to regulate anchorage dependency without disrupting cell-cell interactions[11]. Furthermore, AST cells maintain a clustered morphology by expressing E-cadherin, suggesting that AST promotes cluster-based metastasis rather than single-cell dissemination[11]. CTC clusters contain multiple junction proteins, including Plakoglobin, ICAM1, CD44, and VCAM1, which enhance CTC survival in circulation[44–47]. In ADCM incubation, we observed increased Plakoglobin and VCAM1 expression, and importantly, CD36 inhibition effectively suppressed cluster formation. Our findings

demonstrate that targeting lipid metabolism via CD36 and CPT1A inhibition effectively suppresses AST and AST-induced metastasis, underscoring the importance of metabolic alterations and lipid uptake during cancer cell dissemination (Fig. 8). Moving forward, we will continue investigating the mechanisms of AST-induced metastasis, focusing on its regulation by lipid metabolism and the antagonistic relationship governing these processes. A deeper understanding of the interactions between cancer cells and the TME will help broaden our knowledge of TME-driven metastasis and support the development of effective therapeutic strategies for clinical application.

Limitations

While our study provides strong evidence for the role of adipocytes in regulating AST and AST-induced metastasis, one limitation is the lack of in vivo validation. However, our primary objective was to unravel the mechanistic aspects of adipocyte-mediated AST regulation under well-controlled in vitro conditions. Given the complexity of TME in vivo, our findings lay a critical foundation for understanding the fundamental processes governing AST. Future studies utilizing in vivo models will be essential to validate our in vitro findings and further explore the physiological relevance of adipocyte-induced AST in metastasis. By bridging the gap between in vitro mechanistic insights and in vivo validation, we aim to deepen our understanding of TME-driven cancer metastasis and identify potential therapeutic targets for clinical application.

Data availability

TCGA data references are on cBioPortal (https://www.cbioportal.org/). Co-expression analysis of lipid transport genes for 17 AST factors was done using data from the GSEA (https://www.gsea-msigdb.org/gsea/index.jsp).

Received: 20 December 2024; Accepted: 23 July 2025
Published online: 20 August 2025

References

1. Dillekås, H., Rogers, M. S. & Straume, O. Are 90% of deaths from cancer caused by metastases? *Cancer Med.* **8**, 5574–5576. https://doi.org/10.1002/cam4.2474 (2019).
2. Swartz, M. A. et al. Tumor microenvironment complexity: emerging roles in cancer therapy. *Cancer Res.* **72**, 2473–2480. https://doi.org/10.1158/0008-5472.Can-12-0122 (2012).
3. Joyce, J. A. & Pollard, J. W. Microenvironmental regulation of metastasis. *Nat. Rev. Cancer*. **9**, 239–252. https://doi.org/10.1038/nrc2618 (2009).
4. Mukherjee, A., Bilecz, A. J. & Lengyel, E. The adipocyte microenvironment and cancer. *Cancer Metastasis Rev.* **41**, 575–587. https://doi.org/10.1007/s10555-022-10059-x (2022).
5. Wang, Z. et al. Metastasis-associated fibroblasts: an emerging target for metastatic cancer. *Biomark. Res.* **9** https://doi.org/10.1186/s40364-021-00305-9 (2021).
6. Lin, Y., Xu, J. & Lan, H. Tumor-associated macrophages in tumor metastasis: biological roles and clinical therapeutic applications. *J. Hematol. Oncol.* **12**, 76. https://doi.org/10.1186/s13045-019-0760-3 (2019).
7. Mittal, V. Epithelial mesenchymal transition in tumor metastasis. *Annu. Rev. Pathol.* **13**, 395–412. https://doi.org/10.1146/annurev-pathol-020117-043854 (2018).
8. Yu, M. et al. Circulating breast tumor cells exhibit dynamic changes in epithelial and mesenchymal composition. *Science* **339**, 580–584. https://doi.org/10.1126/science.1228522 (2013).
9. Padmanaban, V. et al. E-cadherin is required for metastasis in multiple models of breast cancer. *Nature* **573**, 439–444. https://doi.org/10.1038/s41586-019-1526-3 (2019).
10. Cheung, K. J., Gabrielson, E., Werb, Z. & Ewald, A. J. Collective invasion in breast cancer requires a conserved basal epithelial program. *Cell* **155**, 1639–1651. https://doi.org/10.1016/j.cell.2013.11.029 (2013).
11. Huh, H. D. et al. Reprogramming anchorage dependency by adherent-to-suspension transition promotes metastatic dissemination. *Mol. Cancer*. **22**, 63. https://doi.org/10.1186/s12943-023-01753-7 (2023).
12. Takahashi, K. & Yamanaka, S. Induction of pluripotent stem cells from mouse embryonic and adult fibroblast cultures by defined factors. *Cell* **126**, 663–676. https://doi.org/10.1016/j.cell.2006.07.024 (2006).
13. Dongre, A. & Weinberg, R. A. New insights into the mechanisms of epithelial–mesenchymal transition and implications for cancer. *Nat. Rev. Mol. Cell Biol.* **20**, 69–84. https://doi.org/10.1038/s41580-018-0080-4 (2019).
14. Brown, K. A. & Scherer, P. E. Update on adipose tissue and cancer. *Endocr. Rev.* **44**, 961–974. https://doi.org/10.1210/endrev/bnad015 (2023).
15. Wu, Q. et al. Cancer-associated adipocytes: key players in breast cancer progression. *J. Hematol. Oncol.* **12**, 95. https://doi.org/10.1186/s13045-019-0778-6 (2019).
16. Choi, J., Cha, Y. J. & Koo, J. S. Adipocyte biology in breast cancer: from silent bystander to active facilitator. *Prog Lipid Res.* **69**, 11–20 (2018).
17. Gyamfi, J. et al. Interaction between CD36 and FABP4 modulates adipocyte-induced fatty acid import and metabolism in breast cancer. *Npj Breast Cancer*. **7**, 129. https://doi.org/10.1038/s41523-021-00324-7 (2021).
18. Nieman, K. M., Romero, I. L., Van Houten, B. & Lengyel, E. Adipose tissue and adipocytes support tumorigenesis and metastasis. *Biochim. Biophys. Acta*. **1831**, 1533–1541. https://doi.org/10.1016/j.bbalip.2013.02.010 (2013).
19. Nieman, K. M. et al. Adipocytes promote ovarian cancer metastasis and provide energy for rapid tumor growth. *Nat. Med.* **17**, 1498–1503. https://doi.org/10.1038/nm.2492 (2011).
20. Pascual, G. et al. Targeting metastasis-initiating cells through the fatty acid receptor CD36. *Nature* **541**, 41–45. https://doi.org/10.1038/nature20791 (2017).
21. Ladanyi, A. et al. Adipocyte-induced CD36 expression drives ovarian cancer progression and metastasis. *Oncogene* **37**, 2285–2301. https://doi.org/10.1038/s41388-017-0093-z (2018).
22. Gyamfi, J., Lee, Y. H., Eom, M. & Choi, J. Interleukin-6/STAT3 signalling regulates adipocyte induced epithelial-mesenchymal transition in breast cancer cells. *Sci. Rep.* **8**, 8859. https://doi.org/10.1038/s41598-018-27184-9 (2018).
23. Huh, H. D. et al. Adherent-suspension plasticity promotes the dissemination and colonization of circulating tumor cells. *bioRxiv*, 2024.2011.2025.625320, (2024). https://doi.org/10.1101/2024.11.25.625320
24. Lee, Y. H., Petkova, A. P., Mottillo, E. P. & Granneman, J. G. In vivo identification of bipotential adipocyte progenitors recruited by β3-adrenoceptor activation and high-fat feeding. *Cell. Metab.* **15**, 480–491. https://doi.org/10.1016/j.cmet.2012.03.009 (2012).
25. Lee, M. J. & Fried, S. K. Optimal protocol for the differentiation and metabolic analysis of human adipose stromal cells. *Methods Enzymol.* **538**, 49–65. https://doi.org/10.1016/b978-0-12-800280-3.00004-9 (2014).

26. Tucci, J. et al. Adipocytes provide fatty acids to acute lymphoblastic leukemia cells. *Front. Oncol.* **11**, 665763. https://doi.org/10.3389/fonc.2021.665763 (2021).
27. Balaban, S. et al. Adipocyte lipolysis links obesity to breast cancer growth: adipocyte-derived fatty acids drive breast cancer cell proliferation and migration. *Cancer Metab.* **5**, 1. https://doi.org/10.1186/s40170-016-0163-7 (2017).
28. Koundouros, N. & Poulogiannis, G. Reprogramming of fatty acid metabolism in cancer. *Br. J. Cancer.* **122**, 4–22. https://doi.org/10.1038/s41416-019-0650-z (2020).
29. Rubtsova, S. N., Zhitnyak, I. Y. & Gloushankova, N. A. Phenotypic plasticity of cancer cells based on remodeling of the actin cytoskeleton and adhesive structures. *Int. J. Mol. Sci.* **22** https://doi.org/10.3390/ijms22041821 (2021).
30. Kurma, K. & Alix-Panabières, C. Mechanobiology and survival strategies of circulating tumor cells: a process towards the invasive and metastatic phenotype. *Front. Cell. Dev. Biology*. https://doi.org/10.3389/fcell.2023.1188499 (2023).
31. Yu, X., Mi, S., Ye, J. & Lou, G. Aberrant lipid metabolism in cancer cells and tumor microenvironment: the player rather than bystander in cancer progression and metastasis. *J. Cancer*. **12**, 7498–7506. https://doi.org/10.7150/jca.64833 (2021).
32. Lee, C. K. et al. Tumor metastasis to lymph nodes requires YAP-dependent metabolic adaptation. *Science* **363**, 644–649. https://doi.org/10.1126/science.aav0173 (2019).
33. Pike, L. S., Smift, A. L., Croteau, N. J., Ferrick, D. A. & Wu, M. Inhibition of fatty acid oxidation by etomoxir impairs NADPH production and increases reactive oxygen species resulting in ATP depletion and cell death in human glioblastoma cells. *Biochim. Biophys. Acta*. **1807**, 726–734. https://doi.org/10.1016/j.bbabio.2010.10.022 (2011).
34. Taftaf, R. et al. ICAM1 initiates CTC cluster formation and trans-endothelial migration in lung metastasis of breast cancer. *Nat. Commun.* **12**, 4867. https://doi.org/10.1038/s41467-021-25189-z (2021).
35. Yipp, B. G. et al. Differential roles of CD36, ICAM-1, and P-selectin in plasmodium falciparum cytoadherence in vivo. *Microcirculation* **14**, 593–602. https://doi.org/10.1080/10739680701404705 (2007).
36. Fares, J., Fares, M. Y., Khachfe, H. H., Salhab, H. A. & Fares, Y. Molecular principles of metastasis: a hallmark of cancer revisited. *Signal. Transduct. Target. Therapy*. **5**, 28. https://doi.org/10.1038/s41392-020-0134-x (2020).
37. Notarnicola, M. et al. Serum lipid profile in colorectal cancer patients with and without synchronous distant metastases. *Oncology* **68**, 371–374. https://doi.org/10.1159/000086977 (2005).
38. Liu, Y. L. et al. Association of serum lipid profile with distant metastasis in breast cancer patients. *Zhonghua Zhong Liu Za Zhi*. **34**, 129–131. https://doi.org/10.3760/cma.j.issn.0253-3766.2012.02.010 (2012).
39. Bergers, G. & Fendt, S. M. The metabolism of cancer cells during metastasis. *Nat. Rev. Cancer*. **21**, 162–180. https://doi.org/10.1038/s41568-020-00320-2 (2021).
40. Wang, Y. et al. CPT1A-mediated fatty acid oxidation promotes colorectal cancer cell metastasis by inhibiting Anoikis. *Oncogene* **37**, 6025–6040. https://doi.org/10.1038/s41388-018-0384-z (2018).
41. Bose, S., Zhang, C. & Le, A. Glucose metabolism in cancer: the Warburg effect and beyond. *Adv. Exp. Med. Biol.* **1311**, 3–15. https://doi.org/10.1007/978-3-030-65768-0_1 (2021).
42. Shivdasani, R. A. et al. Transcription factor NF-E2 is required for platelet formation independent of the actions of thrombopoietin/mgdf in megakaryocyte development. *Cell* **81**, 695–704. https://doi.org/10.1016/0092-8674(95)90531-6 (1995).
43. Guan, L. et al. NFE2L2 mutations enhance radioresistance in head and neck cancer by modulating intratumoral myeloid cells. *Cancer Res.* **83**, 861–874. https://doi.org/10.1158/0008-5472.Can-22-1903 (2023).
44. Schuster, E. et al. Better together: circulating tumor cell clustering in metastatic cancer. *Trends Cancer*. **7**, 1020–1032. https://doi.org/10.1016/j.trecan.2021.07.001 (2021).
45. Aceto, N. et al. Circulating tumor cell clusters are oligoclonal precursors of breast cancer metastasis. *Cell* **158**, 1110–1122. https://doi.org/10.1016/j.cell.2014.07.013 (2014).
46. Küçükköse, E. et al. Lymphatic invasion of Plakoglobin-dependent tumor cell clusters drives formation of polyclonal lung metastases in colon cancer. *Gastroenterology* **165**, 429–444e415. https://doi.org/10.1053/j.gastro.2023.02.047 (2023).
47. Zhang, D. et al. VCAM1 promotes tumor cell invasion and metastasis by inducing EMT and transendothelial migration in colorectal cancer. *Front. Oncol.* **10**, 1066. https://doi.org/10.3389/fonc.2020.01066 (2020).

Acknowledgements

This work was part of research projects funded by the National Research Foundation of Korea (NRF) (2020M3F7A109409421 2020R1A2C100337812 and RS-2024-00509461).

Author contributions

D.K. devised most of the experimental plans and conducted the experiments. H.W.P. provided MDA-MB-231 and SUIT2 cell lines and offered advice on experiments. B.S.M. provided human adipose tissues. J.C., as the corresponding author, participated in experimental design and manuscript writing.

Funding

This work was part of research projects funded by the National Research Foundation of Korea (NRF) (2020M3F7A109409421, 2020R1A2C100337812 and RS-2024-00509461).

Declarations

Ethics approval and consent to participate

Human adipose tissue usage received ethical approval from the Institutional Review Board at Gangnam Severance Hospital, Yonsei University, Seoul, Republic of Korea, adhering to the ethical principles outlined in the 1975 Declaration of Helsinki. Acquisition of human adipose tissue samples was conducted with the informed consent of participating patients, following guidelines and regulations approved by the Institutional Review Board of Gangnam Severance Hospital, Yonsei University Health System.

Consent for publication

All authors have consented to their inclusion in the list and have approved the submission of this content. The material has not been presented for publication elsewhere during the review process for consideration.

Competing interests

The authors declare no competing interests.

Additional information

Supplementary Information The online version contains supplementary material available at https://doi.org/10.1038/s41598-025-13309-4.

Correspondence and requests for materials should be addressed to J.C.

Reprints and permissions information is available at www.nature.com/reprints.

Publisher's note Springer Nature remains neutral with regard to jurisdictional claims in published maps and institutional affiliations.